Applying the Yule-Nielsen equation with negative n

Achim Lewandowski and Marcus Ludl

Austrian Research Institute for Artificial Intelligence
Freyung 6/6, A1010 Vienna, Austria

{*achim, marcus*}*@ofai.at*

Gerald Byrne

SURFACE INSPECTION LTD, Unit 6 St Philips Central,
Albert Rd, Bristol BS2 0XJ, United Kingdom

gerald.byrne@surface-inspection.com

Georg Dorffner

Department of Medical Cybernetics and Artificial Intelligence,
Center for Brain Research,
Medical University of Vienna, Austria,
Freyung 6/2, A1010 Vienna, Austria

georg.dorffner@meduniwien.ac.at

The theory of halftone printing has attracted the attention of both industry and scientists for decades. The Yule-Nielsen equation has been used for color prediction for more than 50 years now, but apparently the tuning parameter n has only been taken to be larger or equal than one. Our paper shows that the extension to the whole real axis is well defined in a mathematical sense. We fitted models to data from the ceramics tile printing sector (Rotocolor$^{\text{TM}}$ and Kerajet$^{\text{TM}}$ printing techniques) and found that using a negative n in almost all considered cases resulted in a better fit.

OCIS codes: 100.2810, 120.5700

1. Introduction and Motivation

Both industrial sectors concerned with printing on paper and printing on tiles use halftone printing techniques. A considerable number of color prediction papers deals with the task of finding a model to describe the result when an ink is applied to a paper via halftone technique. In the ceramics sector the goal is the same: an ink pattern is applied via screen, Rotocolor$^{\text{TM}}$ cylinders or even an inkjet printer (Kerajet$^{\text{TM}}$) to a glazed tile. The assumption that the resulting spectral curve of a halftone pattern is a linear combination of the spectral curves of ink and background (paper or glazed tile) is strongly related to the approach Murray-Davies[1] used. In short, the formula for the resulting spectral reflectance, when an ink is printed onto a background with reflectance curve $R_B(\lambda)$, whereby the nominal halftone is h and the effective halftone is $f(h)$, can be expressed as

$$R(h,\lambda) = f(h)R_I(\lambda) + [1 - f(h)]R_B(\lambda) \tag{1}$$

with $R_I(\lambda)$ denoting the reflectance curve of the ink. For transparent inks the value $R_I(\lambda)$ depends on both ink properties *and* the background.

As the effective halftone might differ from the nominal halftone, a monotonic dot gain transformation function $f(h)$ is used to transform the nominal halftone into the effective halftone to incorporate possible dot gain.

Practical experience showed that this approach was often too imprecise to cope with effects caused by scattering and internal reflections. Approximations for real world data are sometimes not convincing when the Murray-Davies approach is used.

Yule and Nielsen[2] introduced an extension which includes the Murray-Davies formula as a special case with $n = 1$. Omitting the λ notation hereafter:

$$R(h,n) = \left\{ f(h)R_I^{\frac{1}{n}} + [1 - f(h)]R_B^{\frac{1}{n}} \right\}^n \tag{2}$$

Some authors tried to determine the most suitable value of n. Ruckdeschel and Hauser[3] concluded that values of n between 1 and 2 can occur in the framework considered by them. Pearson[4] found that a value of $n = 1.7$ has some optimal properties under certain circumstances. Berns et al.[5] found that optimal Yule-Nielsen factors as large as $n = 10$ can be observed.

The theory of Clapper-Yule[6] also considers internal reflections at the boundary between substrate and air. In recent years several authors have tried to find more and more elaborated *physical* models to explain observed reflectance curves, mainly in the area of printing on paper. Approaches include the extensions of point spread functions to model light scattering or the use of probabilities to model the internal reflection behavior,[7,8] variations of the Kubelka-Munk theory[9,10] or extensions of the Yule-Nielsen modified spectral Neugebauer model.[11]

There are also approaches to use the Yule-Nielsen equation with wavelength-depending factors.[12,13]

We have found that in case of the original Yule-Nielsen equation optimal factors even larger than 10 are not uncommon for tile printing in the ceramics sector. This observation led us to the idea to investigate the limit for $n \to \infty$. Gemeinhardt[14] used also this limit for his approach.

While experimenting with the optimal Yule-Nielsen factor, we noticed that often *negative* factors yield even better approximations. We start with a section about considerations, whether the Yule-Nielsen equation has a physical interpretation and we will outline how we intend to use the Yule-Nielsen equation. In the next section, we will show then that not only the limit of the Yule-Nielsen equation for $n \to +\infty$ exists, but furthermore an extension of the Yule-Nielsen factor 'even beyond infinity' is possible. We work with the reciprocal of the original factor, and the extension can then be seen as the transition from the positive axis to negative values. The following section analyses properties of this transition.

The subsequent section treats a practical problem to determine the optimal factor. We performed extensive trials with different tile types to investigate whether the extension to negative values is useful in practice. The positive results of these experiments are given in the final section.

2. Interpretation of the Yule-Nielsen equation

In this section we start with an investigation, whether it is meaningful to assign a physical interpretation to the involved parameters of the Yule-Nielsen equation, especially if the factor n is negative.

Yang[8] remarks that 'numerous researchers have made great efforts to improve numerical accuracy', but that '... these improvements depend on introducing more Y-N factors in regression processes' and '... do not provide more physical insight into real problems'. Concerning flourescent whitening agents in papers, 'physical interpretations of Y-N factors become even less clear".

Not quite so harsh, Arney and Yamaguchi[15] conclude that the 'Yule-Nielsen equation is not a description of the physical mechanism of halftone imaging, but it is a useful empirical approximation'. Their study indicates that the optimal factor is also influenced by the sharpness of the halftone dot edges and by scattering of light within the ink.

In order to apply the Yule-Nielsen equation we need to determine $f(h)$ and the factor n. If n is assumed to be known, a densitometer measurement could be used to estimate $f(h)$. For the general case Wyble and Burns[16] mention different ways to estimate the effective coverage. They prefer a method, where, separately for each considered n, linear regressions are performed in the space of transformed reflectance curves $R^{1/n}$, yielding an estimate of

$f(h)$ and finally a prediction in the original space of reflectance curves. The best performing n is chosen.

Gemeinhardt[14] assumes, although without further explanation, that the limit of the Yule-Nielsen equation for $n \to \infty$ gives an adequate approximation. Under this assumption he uses an additional densitometer measurement to find an estimator for the involved effective coverage.

We believe, as Arney and Yamaguchi, that the Yule-Nielsen equation is well suited if seen as an instrument to fit a mathematical model to given data, but in our approach the numerical accuracy is improved *without* introducing new parameters. Except for special cases (besides $n = 1$ Yule and Nielsen mention the case $n = 2$, which is related to full scattering), n may have not a direct physical meaning, but qualitative statements as "if n is increased then $R(h, n)$ will decrease", assuming $R_I < R_B$, can still be made. $R(h, n)$ will decrease for $n \to +\infty$ to a limit, which is still larger than R_I. For example, as we will see in the following section, in the case of $f(h) = 0.5$ $R(h, n)$ can never be smaller than the geometric mean $\sqrt{R_I R_B}$.

$R(h, n)$ can be decreased even further by allowing negative values of n. Extending the domain of n to the whole axis allows us to produce values $R(h, n)$ arbitrarily near to R_I. The Yule-Nielsen effect can be made much larger than before, and when n approaches 0 from the negative axis, we could even model the extreme case that inspite of an effective halftone $f(h) < 1$ the reflectance curve R_I of the applied ink is observed.

We are always assuming that the reflectance curves R_I and R_B are known and that we have measured m reflectance curves $S(h_i)$, $i = 1, \ldots, m$, with known nominal halftones h_i, $i = 1, \ldots, m$. We do not have any additional densitometer measurements. Our goal is to approximate all $S(h_i)$ by functions $R(h_i, n)$ using always the same, but so far unknown value of n and possibly different values $f(h_i)$, $i = 1, \ldots, m$:

$$R(h_i, n) = \left\{ f(h_i) R_I^{\frac{1}{n}} + [1 - f(h_i)] R_B^{\frac{1}{n}} \right\}^n \tag{3}$$

We minimize the average distance (Euclidean norm) ΔR between observed and fitted reflectance curves and it should be clear that the chosen error function has an influence onto the fitted parameters. In the general case of unknown $f(h_i)$, $i = 1, \ldots, m$ *and* unknown n we could interpret the estimators of $f(h_i)$ as estimators of effective halftones, although we will never need them explicitly in this sense. In addition, the physical definition of effective halftones is difficult, if the thickness of the applied ink layer is not constant, but slowly approaches zero at the border of the printed dots.

Furthermore, if we assume that n is known, the best estimators of $f(h_i)$ will change. For example, if we would like to test the suitability of the Murray-Davies equation ($n = 1$) then we do not use the estimators of $f(h_i)$ found in the general case, but will calculate new

estimators. Therefore, we cannot speak of *the* effective halftones, but each environment has its own optimal estimators.

3. Limit of Yule-Nielsen equation

As we will see later, it has computational advantages to use the Yule-Nielsen equation in a slightly different form by replacing n by $1/u$:

$$R_*(h,u) = \{f(h)R_I^u + [1-f(h)]R_B^u\}^{\frac{1}{u}} \tag{4}$$

The original Yule-Nielsen equation is used for $1 \leq n < +\infty$, which corresponds to the interval $(0,1]$ for u.

The limit for $u \to 0$ (for fixed h) can be calculated as in the following lemma, which is in fact a simple extension of the limit Pollack[17] derived in 1955:

Lemma 1 *The limit* $\lim_{u\to 0} R_*(h,u)$ *exists and it is*

$$\lim_{u\to 0} R_*(h,u) = R_I^{f(h)} R_B^{1-f(h)}$$

If we write this in the form

$$R_I^{f(h)} R_B^{1-f(h)} = R_B \left(\frac{R_I}{R_B}\right)^{f(h)}, \tag{5}$$

we see that the limit reflectance curve can be interpreted as being generated by light passing twice a transparent layer with transmittance

$$\left(\frac{R_I}{R_B}\right)^{f(h)/2}, \tag{6}$$

whereby the light is reflected once at the background with reflectance curve R_B.

The interesting part is now that we did not make explicit use of the fact that u approaches 0 from the *positive* real axis. In terms of the original form of the Yule-Nielsen equation, we could have taken $\lim_{n\to-\infty}$ as well. The Yule-Nielsen equation behaves identically for very large positive values of n and for negative values with large magnitudes.

Figure 1 shows the functions $R(h,n)$ and $R_*(h,u)$ for the arbitrarily chosen values of $f(h) = 0.3$, $R_I = 0.2$ and $R_B = 0.7$ respectively. The upper graph shows the behavior of $R(h,n)$ as a function of n, the bottom graph uses the new notation displaying $R_*(h,u)$ as a function of u. In this example the asymptotic function value $R(h,n)$ both for $n \to +\infty$ and $n \to -\infty$ is

$$R_I^{f(h)} R_B^{1-f(h)} = 0.2^{0.3} 0.7^{0.7} \approx 0.4807. \tag{7}$$

It can be shown that $\lim_{u\to+\infty} R_* = \max(R_B, R_I)$ and $\lim_{u\to-\infty} R_* = \min(R_B, R_I)$:

Lemma 2 *Assume that* $0 < R_I \leq R_B$*, then* $\lim_{u\to+\infty} R_*(h,u) = R_B$

Proof:

$$\begin{aligned}\lim_{u\to\infty} R_*(h,u) &= \lim_{u\to\infty} \{f(h)R_I^u + [1-f(h)]R_B^u\}^{\frac{1}{u}} &(8)\\ &= \lim_{u\to\infty} R_B\left[f(h)\left(\frac{R_I}{R_B}\right)^u + 1 - f(h)\right]^{\frac{1}{u}} &(9)\\ &= R_B &(10)\end{aligned}$$

The other three possible cases are proven in a similar way. For a given wavelength, every value between R_I and R_B can be generated by changing u, as $R_*(h,u)$ is continuous.

The essence of Lemmas 1 and 2 is that it is possible to define the Yule-Nielsen equation for all real values of n. The limit for $n \to +\infty$ exists, but furthermore it seems natural to continue 'beyond infinity', which means, in the old notation, to switch to negative infinite values. The new notation using u is, for this purpose, more elegant, as we just progress smoothly from the positive axis through 0 to the negative axis.

4. Behavior of the Yule-Nielsen equation around $u = 0$

We investigated further what might happen during the transition of u from the positive to the negative axis. We computed the linear Taylor expansion around $u = 0$ for a fixed h:

Lemma 3 *The linear Taylor expansion for* $R_*(h,u)$ *around* $u = 0$ *is:*

$$A(h,u) = R_I^{f(h)} R_B^{1-f(h)} \left\{1 + \frac{u}{2} f(h)[1-f(h)]\left[\log\left(\frac{R_I}{R_B}\right)\right]^2\right\}$$

Proof:

We need to find the limit of the difference quotient

$$\lim_{u\to 0} \frac{R_*(h,u) - R_*(h,0)}{u-0}, \tag{11}$$

whereby $R_*(h,0)$ is defined as the limit $R_I^{f(h)} R_B^{1-f(h)}$. L'Hopital's Rule tells us to use $\lim_{u\to 0} R'_*(h,u)$ instead, assuming that this limit exists. It is not difficult to see that the derivative of $R_*(h,u)$ with respect to u exists for $u \neq 0$.

Define

$$G(u) := f(h)R_I^u + [1-f(h)]R_B^u, \tag{12}$$

then the k-th derivative can be calculated as

$$G^{(k)}(u) = f(h)\left[\log(R_I)\right]^k R_I^u + [1-f(h)]\left[\log(R_B)\right]^k R_B^u \tag{13}$$

Now for $u \neq 0$

$$R_*(h,u) = \exp\{\frac{1}{u}\log[G(u)]\} \tag{14}$$

and therefore

$$\begin{aligned} R'_*(h,u) &= R_*(h,u)\left\{-\frac{1}{u^2}\log[G(u)] + \frac{1}{u}\frac{G'(u)}{G(u)}\right\} &(15)\\ &= R_*(h,u)\left\{\frac{u\frac{G'(u)}{G(u)} - \log[G(u)]}{u^2}\right\} &(16)\end{aligned}$$

We define

$$H(u) := u\frac{G'(u)}{G(u)} - \log[G(u)] \tag{17}$$

and then it follows

$$\begin{aligned} H'(u) &= \frac{G'(u)}{G(u)} + u\frac{G''(u)G(u) - G'(u)G'(u)}{G^2(u)} - \frac{G'(u)}{G(u)} &(18)\\ &= u\frac{G''(u)G(u) - G'(u)G'(u)}{G^2(u)} &(19)\end{aligned}$$

We consider now the following limit

$$\lim_{u\to 0}\frac{H'(u)}{2u} = \lim_{u\to 0}\frac{G''(u)G(u) - G'(u)G'(u)}{2G^2(u)} \tag{20}$$

Using (12) and (13) we arrive after some calculations at

$$\lim_{u\to 0}\frac{H'(u)}{2u} = \frac{1}{2}f(h)[1-f(h)]\left[\log\left(\frac{R_I}{R_B}\right)\right]^2 \tag{21}$$

After applying L'Hopital's Rule on the second part of (16), we can calculate the desired limit:

$$\lim_{u\to 0} R'_*(h,u) = \frac{1}{2}R_I^{f(h)}R_B^{1-f(h)}f(h)[1-f(h)]\left[\log\left(\frac{R_I}{R_B}\right)\right]^2. \tag{22}$$

Therefore the linear Taylor expansion around $u = 0$ is

$$A(h,u) = R_I^{f(h)}R_B^{1-f(h)}\left\{1 + \frac{u}{2}f(h)[1-f(h)]\left[\log\left(\frac{R_I}{R_B}\right)\right]^2\right\} \tag{23}$$

We can see that the expression $(u/2)f(h)[1-f(h)]\left[\log(R_I/R_B)\right]^2$ describes the relative deviation to the limit $R_*(h,0)$ and is mainly influenced by the two factors $f(h)[1-f(h)]$ and $\left[\log\left(\frac{R_I}{R_B}\right)\right]^2$. Assume that the $f(h)$ is given and that we have two reflectance curves $R_I \leq R_B$. If we alter u now, then, because of the squared logarithm, mainly those wavelenghts are affected, for which $R_I << R_B$. A positive u will lift the resulting reflectance curve in this area, and a negative u will lower it, whereby the areas for which R_I is almost as large as

R_B are not affected to the same extent. In contrast, changing $f(h)$, assuming a small u, will affect more or less the whole range of wavelengths.

Figure 2 shows the behavior of $R_*(h,u)$ for values of $f(h) = 0.52$ and $u \in \{-1, 0, 1\}$ and additionally the observed reflectance curve for a nominal halftone of $h = 0.4$ (R_B, R_I and R_{40} are taken from data set C introduced in the section with the experimental results). Figure 2 shows that allowing a negative u simply extends the function space which can be represented. The variation in the area with high wavelengths (> 600nm) is much lower and each u with $-1 \leq u \leq 0$ might deliver a reasonable fit. For the lower wavelengths, the sensitivity of $R_*(h,u)$ with respect to u is much higher. The observed reflectance curve is lower than expected and can only be expressed with $u < 0$.

5. Determination of best u without a full coverage measurement

For the experimental results presented in the next section we used the measured reflectance curve for a nominal halftone of 100% as R_I, although apparently a full coverage was not achieved. We will show briefly that this property does not hinder the calculation of the best fitting Yule-Nielsen factor u:

Lemma 4 *Suppose that the extended Yule-Nielsen equation describes for a certain u the true situation: each reflectance curve $R_*(h)$ can be expressed either as*

$$R_*(h) = \{f(h)R_I^u + [1 - f(h)]R_B^u\}^{\frac{1}{u}}$$

or as

$$R_*(h) = R_I^{f(h)} R_B^{1-f(h)}$$

depending on whether u is different from zero or not.

If R_I can not be measured, but only a spectral curve for a patch with the maximal available nominal halftone h_0 with $0 < f(h_0) < 1$, we could use $R_{I_0} := R_*(h_0)$ instead, and for each h with $0 < h < h_0$ we will still get a modified Yule-Nielsen equation using the same u as before:

$$R_*(h) = \left\{g(h)R_{I_0}^u + [1 - g(h)]R_B^u\right\}^{\frac{1}{u}}, \quad u \neq 0$$

or

$$R_*(h) = R_{I_0}^{g(h)} R_B^{1-g(h)}, \quad u = 0$$

$g(h)$ is still monotonic.

Proof:

1. Suppose first that a $u \neq 0$ describes the true situation. If

$$R_*(h) = \{f(h)R_I^u + [1 - f(h)]R_B^u\}^{\frac{1}{u}}, \tag{24}$$

then

$$R_{I_0} := R_*(h_0) = \{f(h_0)R_I^u + [1 - f(h_0)]R_B^u\}^{\frac{1}{u}}, \tag{25}$$

We can solve for R_I^u:

$$R_I^u = \frac{1}{f(h_0)}R_{I_0}^u - \frac{1 - f(h_0)}{f(h_0)}R_B^u \tag{26}$$

Substituting in the original equation yields:

$$\begin{aligned}
R_*(h) &= \left\{f(h)\frac{1}{f(h_0)}R_{I_0}^u - \frac{f(h)[1 - f(h_0)]}{f(h_0)}R_B^u + [1 - f(h)]R_B^u\right\}^{\frac{1}{u}} && (27)\\
&= \left(\frac{f(h)}{f(h_0)}R_{I_0}^u + \left\{1 - f(h) - \frac{f(h)[1 - f(h_0)]}{f(h_0)}\right\}R_B^u\right)^{\frac{1}{u}} && (28)\\
&= \left(\frac{f(h)}{f(h_0)}R_{I_0}^u + \left\{1 - \frac{f(h)f(h_0) + f(h)[1 - f(h_0)]}{f(h_0)}\right\}R_B^u\right)^{\frac{1}{u}} && (29)\\
&= \left(\frac{f(h)}{f(h_0)}R_{I_0}^u + \left\{1 - \frac{f(h)}{f(h_0)}\right\}R_B^u\right)^{\frac{1}{u}} && (30)
\end{aligned}$$

Setting $g(h) := f(h)/f(h_0)$ completes the proof for the first case.

2. Suppose that $u = 0$ is optimal. Therefore

$$R_*(h) = R_I^{f(h)}R_B^{1-f(h)} \tag{31}$$

and

$$R_{I_0} := R_*(h_0) = R_I^{f(h_0)}R_B^{1-f(h_0)} \tag{32}$$

and therefore

$$R_I = \left(\frac{R_{I_0}}{R_B^{1-f(h_0)}}\right)^{\frac{1}{f(h_0)}} \tag{33}$$

Substituting yields

$$\begin{aligned}
R_*(h) &= R_I^{f(h)}R_B^{1-f(h)} && (34)\\
&= \left(\frac{R_{I_0}}{R_B^{1-f(h_0)}}\right)^{\frac{f(h)}{f(h_0)}} R_B^{1-f(h)} && (35)\\
&= R_{I_0}^{\frac{f(h)}{f(h_0)}} R_B^{1-f(h)-(1-f(h_0))\frac{f(h)}{f(h_0)}} && (36)\\
&= R_{I_0}^{\frac{f(h)}{f(h_0)}} R_B^{1-\frac{f(h)}{f(h_0)}} && (37)
\end{aligned}$$

As in the first case, setting $g(h) := f(h)/f(h_0)$ completes the proof.

If we believe that the extended Yule-Nielsen equation is an adequate description of the reality, we will therefore be able to determine the optimal u even if we have not observed the reflectance curve R_I itself.

6. Experimental Results

6.A. Description of Experiments

We have investigated whether the extension of the original Yule-Nielsen factor to infinity and further more to the whole set of real numbers yields any benefit, if the optimal factor for *real* data is sought.

We will present results for different tile types. For each tile type one printing layer was applied to a uniform glazed tile. We calculated the distance between observed and fitted reflectance curves a) as a Euclidean distance between the curves and b) as the distance in the CIELAB space.

We proceeded in the following way: All used tile types had patterns with different nominal halftones and unprinted areas. For each tile type the reflectance curve R_B of an unprinted part of a glazed tile was measured. Additionally we measured the reflectance curves for small patches with given nominal halftones (which were $0.20, 0.40, 0.60, 0.80, 1.00$ for data sets A and C, and 0.10, 0.20, ..., 1.00 for data set B). Each single patch with constant halftone had a dimension of at least 2cm x 2cm. If a nominal halftone appeared several times on a tile, we used the average reflectance curve for all available patches of all tiles produced under the same circumstances. The average reflectance curve of the patches with $h = 1.00$ was used as R_I.

6.B. Data set A

Data set A belongs to a black ink pattern printed on a bright glaze and the used nominal halftones are $0, 0.2, 0.4, 0.6, 0.8, 1$. The data can be further split into four groups related to the viscosity of ink (four values of 18s, 20s, 25s and 30s according to the Ford Cup system). The analysis was performed for each of these groups separately. We had the possibility to measure between 3 and 5 tiles for each viscosity both pre and post kiln. The reflectance curve for a given nominal halftone was calculated from all tiles.

We considered the following models:

1. Murray Davies $u = 1$ $(n = 1)$
2. Yule-Nielsen $u = 0$ $(n = +\infty, n = -\infty)$
3. Yule-Nielsen $u < 0$ $(n < 0)$
4. Yule-Nielsen $u > 0$ $(n > 0)$

We took the measured reflectance curve of glaze (nominal halftone=0.00) and the reflectance curve of the nominal 100%-patch as given. If u is already determined (cases 1. and 2.), we estimated $f(0.2), f(0.4), f(0.6)$ and $f(0.8)$. When also u needed to be determined

(cases 3. and 4.), we simultaneously optimized the parameters $f(0.2), f(0.4), f(0.6)$ and $f(0.8)$ and u in order to predict the reflectance curves belonging to the halftones. We used the Nelder-Mead[18] approach implemented in MATLAB with several random starting points and controlled the results by visual inspection of observed and fitted reflectance curves. We tried to minimize the average distance (Euclidean norm) ΔR between observed and fitted reflectance curves. Furthermore, we calculated the mean ΔE_{ab}-distance in the CIELAB space for observed and fitted reflectance curves.

The pre kiln results are summarised in Table 1.

Although even the Murray-Davies equation does perform well, as even in the worst case the average ΔE_{ab} is still only 0.35, a negative value of u performs equally well or better in comparison to a large n. If the best parameter is negative, then for our examples (also for data sets B and C) the best positive u was arbitrarily near to 0, and similar, if the best parameter u was positive, the best negative u was very close to 0.

The post kiln results are summarised in Table 2. They show that using a negative Yule-Nielsen u yields far better results than a non-negative u. The ΔE_{ab} is always below 0.21, whereas the best non-negative u leads to errors that are near 1 in the worst case. The best values of u are always in the range from -1 to -0.7.

The figures 3, 4 and 5 show the poor fit of reflectance curves for the Murray-Davies equation, the fit for $u = 0$ and the excellent fit for the best negative u value. The figures are given for the post kiln results of the ink with viscosity=$25s$.

6.C. Data set B

For the second data set, a Kerajet$^{\text{TM}}$ink jet printer was used. The pattern has different nominal halftones $(0.00, 0.10, 0.20, \ldots, 1.00)$. For each run, the pattern was printed with one of the four colors C, M, Y and K. The tiles were inspected only after the kiln. Table 3 summarizes the results.

Again the best values (ΔR) are achieved when a *negative* u is used. The ΔE_{ab} values for negative u are at least in the same range or better than the remaining values (remember that the parameters were chosen to minimize ΔR). For comparison, we repeated the optimization for data set B, but this time the task was to minimize ΔE_{ab}. The results in Table 4 show that in three of four cases the best results have been achieved with a negative Yule-Nielsen factor. In case of the black ink, the negative factor yields by far the best result.

6.D. Data set C

The tiles for this data set C had patches with nominal halftones of 0.00, 0.20, 0.40, 0.60, 0.80 and 1.00. The pattern was printed with each of two inks, a red and a blue-green. The tiles were measured after firing. Table 5 gives the results.

Again, negative values yielded the best results. Figure 6 shows the near-perfect fit for the red ink.

7. Conclusion

We have shown that the Yule-Nielsen equation can provide substantially improved predictions for reflectance curves of printed tile patterns, if it is used with a negative Yule-Nielsen factor. It is computationally easier to work with the reciprocal of the original factor. Even the limit of the Yule-Nielsen equation for $n \to \infty$ often yields a good performance and could be used instead of a finite positive n.

As the domain of the Yule-Nielsen equation has been extended without increasing the complexity of the calculation, it seems to be reasonable to always include the investigation of negative factors.

In future, we plan to relate the fitted parameters (u and the fitted $f(h)$) to the ink properties as viscosity or density in order to develop a color prediction model integrating the ink properties.

Acknowledgments

This research has been done within the project 'MONOTONE', funded by the European Community in the 'Competitive and Sustainable Growth Programme', under contract number G1RD-CT2002-00783.

The Austrian Research Institute for Artificial Intelligence is supported by the Austrian Federal Ministry for Education, Science and Culture and by the Austrian Federal Ministry of Transport, Innovation and Technology.

We would like to thank Antonio Querol from FERRO, Spain, for providing the reflectance curve measurements for data set B and Guillermo Peris Fajarnes, Technical University of Valencia, for providing the spectrophotometer to facilitate the measurements of data set A.

References

1. A. Murray, "Monochrome reproduction in photoengraving," Journal of the Franklin Institute **221**, 721–744 (1936).
2. J. Yule and W. Nielsen, "The penetration of light into paper and its effect on halftone reproduction," in *TAGA Proc.*, vol. 3, pp. 65–76 (1951).
3. F. Ruckdeschel and O. Hauser, "Yule-Nielsen effect in printing: a physical analysis," Applied Optics **17**(21), 3376–3383 (1978).
4. M. Pearson, "n value for general conditions," in *TAGA Proceedings*, pp. 415–425 (1980).

5. R. Berns, A. Bose, and D. Tzeng, "The spectral modeling of large-format ink jet printers," Research and Development Final Report, RIT Munsell Color Science Laboratory (1996).
6. F. Clapper and J. Yule, "The effect of multiple internal reflections on the densities of halftone prints on paper," Journal of the Optical Society of America **43**, 600–603 (1953).
7. L. Yang, R. Lenz, and B. Kruse, "Light scattering and ink penetration effects on tone reproduction," Journal of the Optical Society of America A **18**(2), 360–366 (2001).
8. L. Yang, "A unified model of optical and physical dot gain in print color reproduction," Journal of Imaging Science and Technology **48**(4), 347–353 (2004).
9. L. Yang and B. Kruse, "Revised Kubelka-Munk theory. I. Theory and application," Journal of the Optical Society of America A **21**(10), 1933–1941 (2004).
10. P. Emmel and R. Hersch, "Towards a color prediction model for printed patches," IEEE Computer Graphics and Applications **19**(4), 54–60 (1999).
11. R. Hersch and F. Crete, "Improving the Yule-Nielsen modified spectral Neugebauer model by dot surface coverages depending on the ink superposition conditions," in *IS & T/SPIE Electronic Imaging Symposium, Conf. Imaging X: Processing, Hardcopy and Applications, Jan. 05, SPIE Vol. 5667*, pp. 434–445 (2005).
12. K. Iino and R. Berns, "Building color management modules using linear optimization. I. Desktop color system," Journal of Imaging Science and Technology **42**, 79–94 (1998).
13. K. Iino and R. Berns, "Building color management modules using linear optimization. II. Prepress system for offset printing," Journal of Imaging Science and Technology **42**, 99–114 (1998).
14. J. Gemeinhardt, "Colorimetric Description of Tolerances in Newspaper Production," in *IARIGAI 2004: Advances in Printing Science and Technology,* vol. 31, pp. 7/1–7/9 (2004).
15. J. Arney and S. Yamaguchi, "The physics behind the Yule-Nielsen equation," in *PICS 1999: Image Processing, Image Quality, Image Capture, Systems Conference*, Savannah, Georgia, pp. 381–385 (1999).
16. D. Wyble and R. Berns, "A critical review of spectral models applied to binary color printing," Color Research and Application **25**1, 4–19 (2000).
17. F. Pollack, "The relationship between the densities and dot sizes of multi-colour halftone images," Journal of Photographic Science, The Royal Photographic Society, London, **3**(4), 112-116 (1955).
18. J. Nelder and R. Mead, "A simplex method for function minimization," Computer Journal **7**(3), 308–313 (1965).

Figures and tables

Figure 1: (a) The function $R(h, n)$ for $f(h) = 0.3$, $R_I = 0.2$ and $R_B = 0.7$. (b) $R_*(h, u)$ for the same parameters.

Figure 2: The function $R_*(h, u)$ for $f(h) = 0.52$ and $u \in \{-1, 0, 1\}$, together with the observed reflectance curve for a nominal halftone $h = 0.4$ (Example from data set C).

Figure 3: Data set A: The fitted reflectance curves (viscosity=25s) for nominal halftones $0.2, 0.4, 0.6$ and 0.8 with the Murray-Davies equation.

Figure 4: Data set A: The fitted reflectance curves (viscosity=25s) for nominal halftones $0.2, 0.4, 0.6$ and 0.8 with the Yule-Nielsen equation ($u = 0$).

Figure 5: Data set A: The fitted reflectance curves (viscosity=25s) for nominal halftones $0.2, 0.4, 0.6$ and 0.8 with the Yule-Nielsen equation (best $u < 0$).

Figure 6: Data set C: The fitted reflectance curves for a red ink pattern printed with a Rotocolor$^{\text{TM}}$.

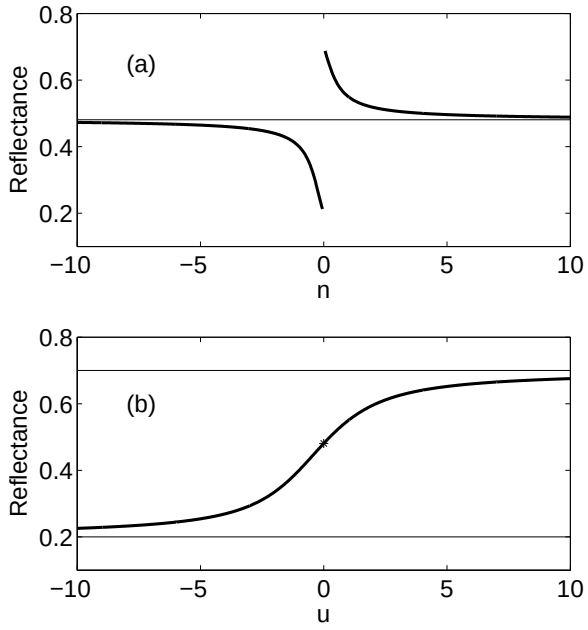

Fig. 1. (a) The function $R(h, n)$ for $f(h) = 0.3$, $R_I = 0.2$ and $R_B = 0.7$. (b) $R_*(h, u)$ for the same parameters. lewandowskifig1.eps

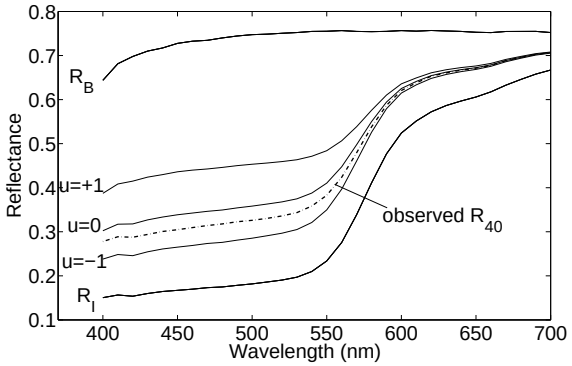

Fig. 2. The function $R_*(h, u)$ for $f(h) = 0.52$ and $u \in \{-1, 0, 1\}$, together with the observed reflectance curve for a nominal halftone $h = 0.4$. (Example from data set C). lewandowskifig2.eps

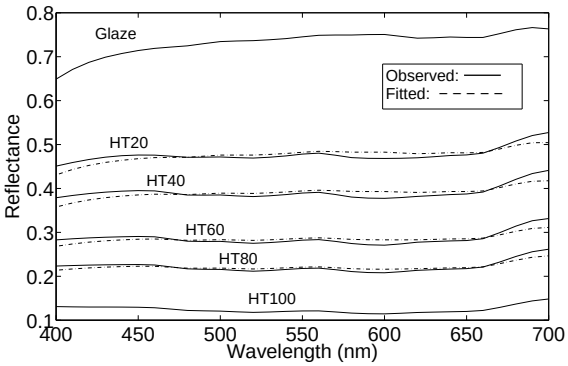

Fig. 3. Data set A: The fitted reflectance curves (viscosity=25s) for nominal halftones $0.2, 0.4, 0.6$ and 0.8 with the Murray-Davies equation. lewandowski-fig3.eps

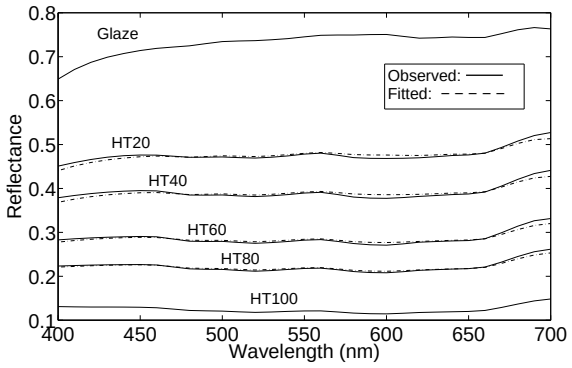

Fig. 4. Data set A: The fitted reflectance curves (viscosity=25s) for nominal halftones $0.2, 0.4, 0.6$ and 0.8 with the Yule-Nielsen equation ($u = 0$). lewandowskifig4.eps

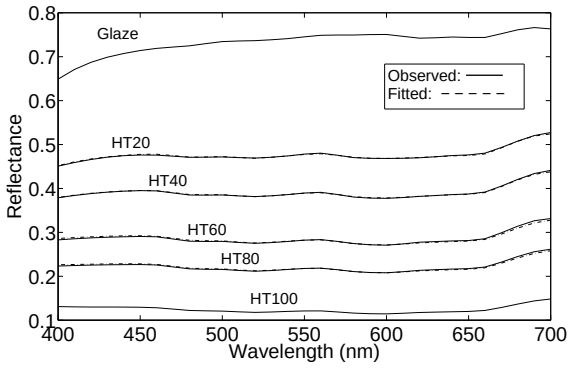

Fig. 5. Data set A: The fitted reflectance curves (viscosity=25s) for nominal halftones $0.2, 0.4, 0.6$ and 0.8 with the Yule-Nielsen equation (best $u < 0$). lewandowskifig5.eps

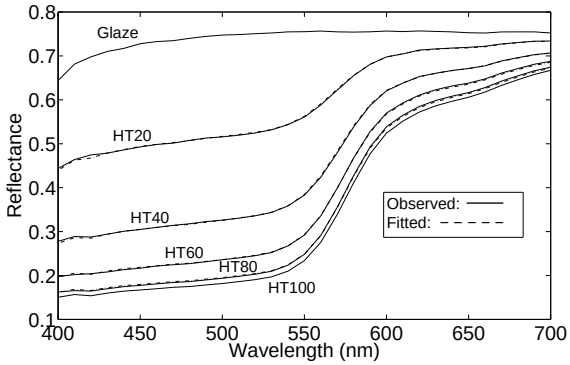

Fig. 6. Data set C: The fitted reflectance curves for a red ink pattern printed with a Rotocolor$^{\mathrm{TM}}$. lewandowskifig6.eps

Table 1. Data set A: Results for a black ink printed on a bright glaze, pre kiln.

Description	Mu-Da	Y-N $u = 0$	Y-N $u \neq 0$
Visc=18s, pre kiln			
best parameter u	1	0	-0.49
$100\Delta R$	1.41	0.57	0.35
ΔE_{ab}	0.29	0.09	0.03
Visc=20s, pre kiln			
best parameter u	1	0	-0.13
$100\Delta R$	1.39	0.41	0.38
ΔE_{ab}	0.30	0.04	0.05
Visc=25s, pre kiln			
best parameter u	1	0	-0.0035
$100\Delta R$	1.44	0.33	0.33
ΔE_{ab}	0.32	0.05	0.05
Visc=30s, pre kiln			
best parameter u	1	0	0.05
$100\Delta R$	1.47	0.29	0.28
ΔE_{ab}	0.35	0.04	0.02

Table 2. Data set A: Results for a black ink printed on a bright glaze, post kiln.

Description	Mu-Da	Y-N $u = 0$	Y-N $u \neq 0$
Visc=18s, post kiln			
best parameter u	1	0	-0.72
$100\Delta R$	4.01	1.94	0.91
ΔE_{ab}	1.04	0.38	0.21
Visc=20s, post kiln			
best parameter u	1	0	-0.80
$100\Delta R$	4.64	2.27	0.78
ΔE_{ab}	1.37	0.55	0.19
Visc=25s, post kiln			
best parameter u	1	0	-0.88
$100\Delta R$	4.99	2.58	0.82
ΔE_{ab}	1.68	0.75	0.18
Visc=30s, post kiln			
best parameter u	1	0	-1.02
$100\Delta R$	5.23	2.85	0.85
ΔE_{ab}	1.98	1.00	0.12

Table 3. Data set B: Post kiln results for the ink jet printer KERAJET^{TM}, if ΔR is minimized.

Description	Mu-Da	Y-N $u = 0$	Y-N $u \neq 0$
Cyan, post kiln			
best parameter u	1	0	-0.43
$100\Delta R$	1.42	0.92	0.86
ΔE_{ab}	0.37	0.28	0.31
Magenta, post kiln			
best parameter u	1	0	-0.25
$100\Delta R$	6.09	1.88	1.41
ΔE_{ab}	2.94	0.68	0.44
Yellow, post kiln			
best parameter u	1	0	-0.72
$100\Delta R$	2.75	1.47	1.10
ΔE_{ab}	0.32	0.28	0.31
Black, post kiln			
best parameter u	1	0	-0.17
$100\Delta R$	5.78	1.62	1.25
ΔE_{ab}	4.45	1.07	0.43

Table 4. Data set B: Post kiln results for the ink jet printer KERAJET^{TM}, if ΔE_{ab} is minimized.

Description	Mu-Da	Y-N $u = 0$	Y-N $u \neq 0$
Cyan, post kiln			
best parameter u	1	0	0.32
$100\Delta R$	1.83	1.26	1.40
ΔE_{ab}	0.27	0.21	0.19
Magenta, post kiln			
best parameter u	1	0	-0.17
$100\Delta R$	10.08	2.69	1.81
ΔE_{ab}	1.85	0.44	0.33
Yellow, post kiln			
best parameter u	1	0	-1.78
$100\Delta R$	2.83	1.63	2.34
ΔE_{ab}	0.27	0.20	0.11
Black, post kiln			
best parameter u	1	0	-0.24
$100\Delta R$	6.74	1.63	1.35
ΔE_{ab}	4.39	1.07	0.30

Table 5. Data set C: Results for the Rotocolor^{TM}, post kiln.

Description	Mu-Da	Y-N $u = 0$	Y-N $u \neq 0$
Red, post kiln			
best parameter u	1	0	-0.40
$100\Delta R$	8.09	2.71	1.02
ΔE_{ab}	2.63	0.91	0.30
Blue-Green, post kiln			
best parameter u	1	0	-0.25
$100\Delta R$	5.37	3.85	3.58
ΔE_{ab}	1.55	1.21	1.15